High-performance electron-transport-layer-free quantum junction solar cells with improved efficiency exceeding 10 %

Yuwen Jia,[†, #] *Haibin Wang,*[‡,#] *Yinglin Wang,*[*, †] *Naoyuki Shibayama,*[§] *Takaya Kubo,*[‡] *Yichun Liu,*[†] *Xintong Zhang,*[*, †] *Hiroshi Segawa*[*, ‡, §]

[†]Center for Advanced Optoelectronic Functional Materials Research, and Key Laboratory of UV Light-Emitting Materials and Technology of Ministry of Education, Northeast Normal University, Changchun 130024, Jilin. P.R. China

[‡]Research Center for Advanced Science and Technology, The University of Tokyo, 153-8904 Tokyo, Japan

[§]Graduate School Arts and Sciences, The University of Tokyo, 153-8902 Tokyo, Japan

[#] Y.J and H.W. contributed equally.

Experimental method

Materials: Ammonium acetate (97.0%), butylamine (Wako Special Grade, Reagent), znic acetate dehydrate (99%), N, N-Dimethylformanide (DMF, Super Dehydrate, Reagent), toluene (Super Dehydrate, 99.50%), octane (Wako Special Grade), acetone (Super Dehydrate) and acetonitrile (Super Dehydrate, 99.80%) were purchased from Wako. Lead bromide ($PbBr_2$, for perovskite precursor, 99%), lead iodide (PbI_2, for perovskite precursor, 99.99%), 2-Methoxyethanol (GR, >99.0%), 2-Aminoethanol (GR, >99.0%), 1,2-Ethanedithiol (>99.0%), Oleic Acid (OA, >85%) and 1-Octadecene (ODE, >90.0%) were purchased from TCI. Lead oxide (PbO, 100.00%) and Hexamethyldisilathiane ($(TMS)_2S$, synthesis Grade) were purchased from Aldrich. Fluorine-doped tin oxide (FTO) glass with a sheet resistance of 10 ohm/square from Nippon sheet glass co. Ltd. was employed as transparent conductive substrate. All the chemicals were not reprocessed.

Solution phase ligand exchange method: The synthesis of oleic-acid-capped CQDs was same as previously studies.[1] The ligand-exchanged precursor solution was prepared by dissolved PbI_2 (0.1 M), $PbBr_2$ (0.05 M) and acetate ammonium (0.04M) in 5 ml DMF. Then mixing 5 ml CQDs solution (octane, 10 mg/ml) with the precursor solution. After stirring vigorously, the CQDs was completely transferred from octane to DMF. The ligand-exchanged solution was washed by octane 3 times, and precipitated by toluene and centrifuge. After drying by argon gas flow, the CQDs was dissolved by butylamine of 200 mg/ml.

Preparation of the CQDSCs: FTO was ultrasonically cleaned three times by detergent, ultra-pure water and ethanol, respectively. The sol-gel ZnO precursor solution was dissolved zinc

acetate (0.55 g) and ethanol amine (100 μl) in 10 ml methanol. The precursor solution was spin-coated on FTO at 3000 rpm for 30 s, then annealed at 350 ℃. The PbS-PbI_2 solution was then spin-coated on the FTO or FTO/ZnO substrate at 1000 rpm for 30 s, following by an annealing on 80 ℃ hotplate in dry room.[2] P-type CQDs was filmed by layer-by-layer method. 50 mg/ml CQDs solution was spin-coated at 2500 rpm for 15 s. Then 1,2-Ethanedithiol (EDT) acetonitrile solution (0.02 vol%) treated the film for 30s, followed by acetonitrile washing 3 times. Finally, 100 nm Au was deposited as the electrode.

Ultraviolet photoelectron spectroscopy (UPS) equipped with He-I source (hv = 21.22 eV) (KRATOS Nova, Shimazu Co.) was used to determine the work function and Fermi level. The level of the samples was referred to that of Au which was in electrical contact with a sample. All measurements were performed under the same negative bias of 6 V.

We estimated the Fermi level (E_F) and the valence band maximum (E_v) of PbS CQDs with respect to vacuum level using UPS (Figure S1a). The conduction band minimum (E_c) of PbS CQDs could be approximated through equation 1

$$E_c = E_v - E_g = E_v - E_{g,opt} - 1.786\frac{e^2}{4\pi\varepsilon_0\varepsilon_{CQD}R} \quad (1)$$

where e is elementary charge, ε_0 is vacuum permittivity, R and $E_{g,opt}$ are the radius and optical bandgap of CQDs, respectively, and ε_{CQD} is the optical dielectric constant of CQD core material which in the used as 17.2 according the reported literature.[3]

Uv-visible near infrared absorption spectrum was measured by HITACHI U4150.

space-charge-limited current (SCLC) measurement was measured by Keithley 2400 soure meter with an electron-type device (FTO/ZnO/PbS/Al). The electron mobility (μ_e) can be calculated by

$$J_D = \frac{9\varepsilon_{CQD}\varepsilon_0\mu V^2}{8L^3}$$

Where L is the thickness of PbS films (250 nm). And the n_{trap} can be calculated by

$$n_{trap} = \frac{2\varepsilon_{CQD}\varepsilon_0 V_{TFL}}{eL^2}$$

The V^2 and V_{TFL} are shown in SCLC plot (Figure S2).

Scanning electron microscope images were captured through HITACHI SU8000.

Current density–voltage (*J*–*V*) characteristic was measured by Keithley 2401 soure meter under simulated 100 mW/cm^2, AM1.5G illumination (BUNKOKEIKI Otento-sun VI). The area of illumination was 0.049 cm^2 with a 2.5mm diameter photo mask, and the step of voltage was 5 mV.

External quantum efficiency (EQE) was BUNKOKEIKI CEP-2000. The area of illumination was 0.049 cm^2, and the step of wavelength was 5 nm.

Light intensity dependency of J_{sc} and V_{oc}. We can analysis the exponential factor (α) from J_{sc} vs light intensity (P) test, using the relational expression of $J_{sc} \propto P^{\alpha}$. The ideal factor (n) and reverse saturation current density (J_0) can be expressed by

$$V_{oc} = \frac{nkT}{q}\ln\left(\frac{J_{sc}}{J_0}\right),$$

where k is Boltzmann constant, T is temperature, and q is elementary charge.

Mott-schokttey measurement was measured by Modulab XM PhotoEchem station (Solartron Analytical). The frequence was 1000 Hz, and the step of voltage was 5 mV.

The depletion width can be expressed by

$$W_D = \frac{1}{N_P}\sqrt{\frac{2\varepsilon\varepsilon_0(V_{bi}-V)}{q(\frac{1}{N_p}-\frac{1}{N_n})}}$$

where N_p and N_n are doping density of PbS-EDT and PbS-PbI_2, ε_0 is vacuum dielectric constant, ε is relative dielectric constant, and V_{bi} is built in potential.

The doping density of PbS-EDT and PbS-PbI_2, was measured by the capacitance–voltage (C–V) curve (Figure S3). The structure of device was FTO/ZnO/CQD/Au, and the equation was

$$\frac{1}{c^2} = \frac{2(V_{bi}-V)}{A^2 q \varepsilon_{CQD}\varepsilon_0 N}$$

where the A was the area of electrode, V_{bi} was the built-in potential, and N was the doping density of PbS-PbI_2 ($N_{PbS\text{-}PbI2}$) and PbS-EDT ($N_{PbS\text{-}EDT}$). The calculated $N_{PbS\text{-}PbI2}$ and $N_{PbS\text{-}EDT}$ are 1.13×10^{16} cm^{-3} and 1.46×10^{16} cm^{-3}.

The variation of J_{sc} and V_{oc} as the function of light-soaking time was measured by Keithley 2400 soure meter under simulated 100 mW/cm^2, AM1.5G illumination (Enlitech, SS-F5-3A) in air ambient environment with the humidity of 30 %.

Table S1. Previous works of the quantum junction solar cells.

Ref	Subject	Device structure	Process	PCE (%)
4	First quantum junction solar cells	ITO/PbS-OH/PbS-I/Al	Layer-by-layer method; Inert atmosphere; Long-time annealing.	5.4
5	Ag-doped p-type PbS	ITO/PbS-OH/PbS-I/AZO	Layer-by-layer method; Inert atmosphere; hot injection Ag doped procedure.	6.1
6	Solution-phase passivation of n-type PbS	ITO/PbS-OH/PbS-I/AZO/Ag	Solution-phase passivation; dip-coating; Inert atmosphere; Long-time annealing.	6.6
7	Graded doping structure	ITO/PbS-OH/PbS-Br/ PbS-I/AZO/Ag	Layer-by-layer; Inert atmosphere.	7.4
This work	Well-passivated and high-quality PbS QDs by ligand engineering.	FTO/PbS-PbI_2/PbS-EDT/Au	Solution-phase ligand exchange; layer-by-layer; **Atmosphere**	10.5

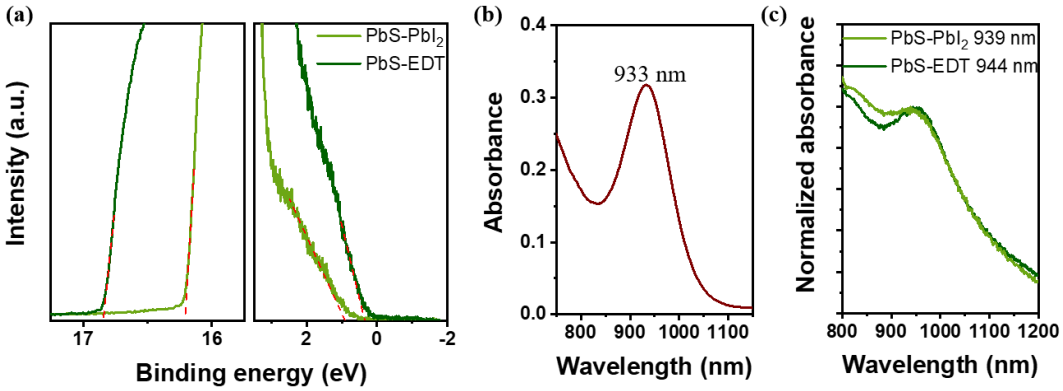

Figure S1. (a)UPS spectra of PbS-PbI_2 and PbS-EDT CQDs. The left side is the secondary electron cut-off region, and the right side is the near Fermi edge. (b) Absorbance spectrum of PbS-OA CQD in octane solution. (c) Normalized absorbance spectrum of PbS-PbI_2 and PbS-EDT films.

Table S2. Energy levels of PbS-PbI_2 and PbS-EDT CQDs measured by UPS and ultraviolet–visible spectroscopy test.

	E_c (eV)	E_v (eV)	E_F (eV)	E_{cutoff} (eV)	E_F-E_V (eV)
PbS-PbI_2	-4.54	-5.91	-5.01	16.21	0.90
PbS-EDT	-3.36	-4.73	-4.37	16.85	0.36

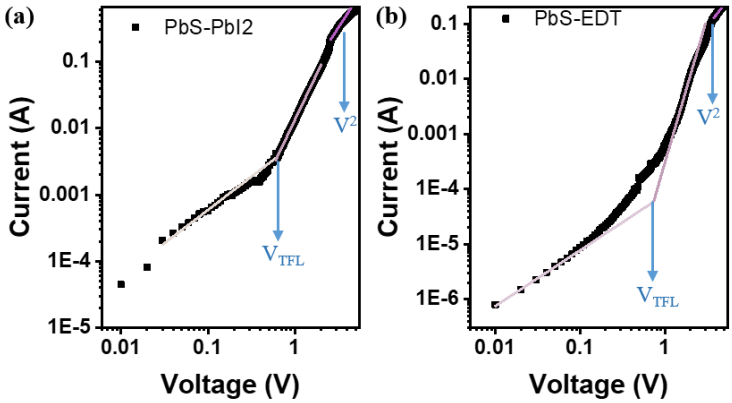

Figure S2. Space-charge-limited current (SCLC) plots of (a) PbS-PbI_2 and (b) PbS-EDT film.

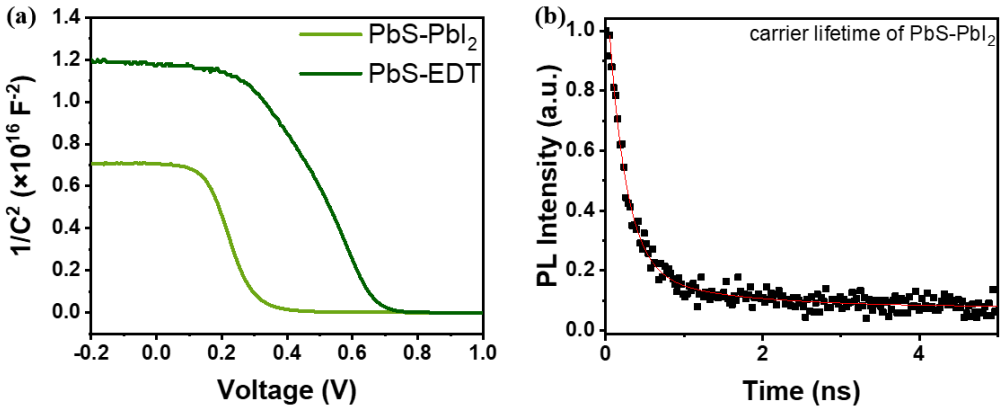

Figure S3. (a) Mott–Schottky plot of PbS-PbI_2 and PbS-EDT with structure of FTO/ZnO/PbS/Au. (b) PL decay trace of PbS-PbI_2 film.

Table S3. Photoelectrical properties of the PbS-PbI_2 and PbS-EDT films.

	μ_e (cm^2/V S)	n_{trap} (cm^{-3})	N (cm^{-3})	τ (ns)
PbS-PbI_2	2.77×10^{-3}	1.91×10^{16}	1.13×10^{16}	0.769
PbS-EDT	7.76×10^{-4}	2.24×10^{16}	1.46×10^{16}	

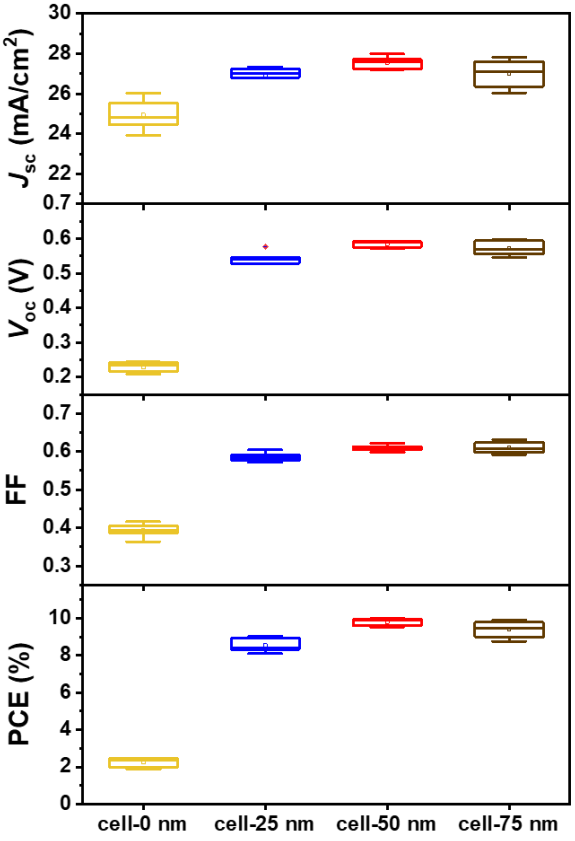

Figure S4. Performance parameters of QJSCs with different thickness of PbS-EDT.

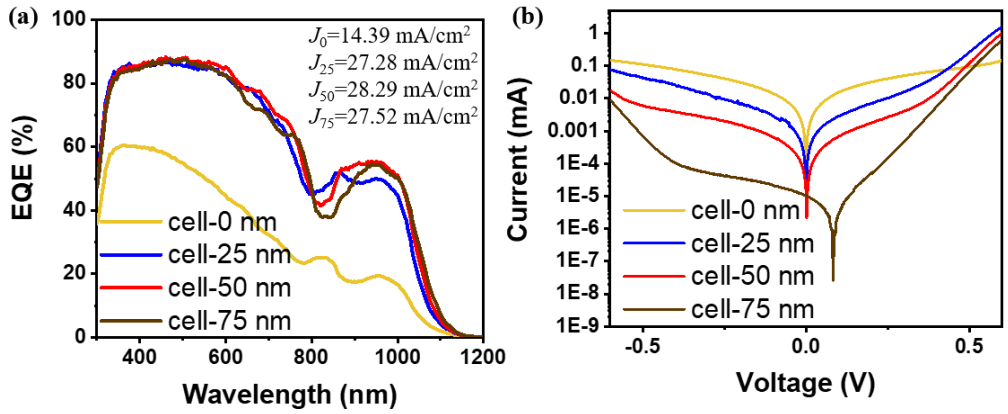

Figure S5. (a) EQE curves for devices with different thickness of PbS-PbI_2. (b) *J–V* characteristics in the dark of these devices.

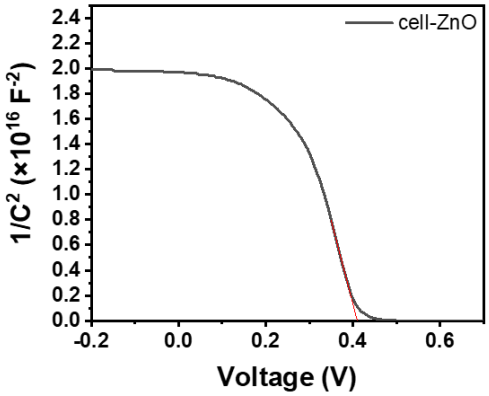

Figure S6. Mott-Schottky plot of cell-ZnO devices

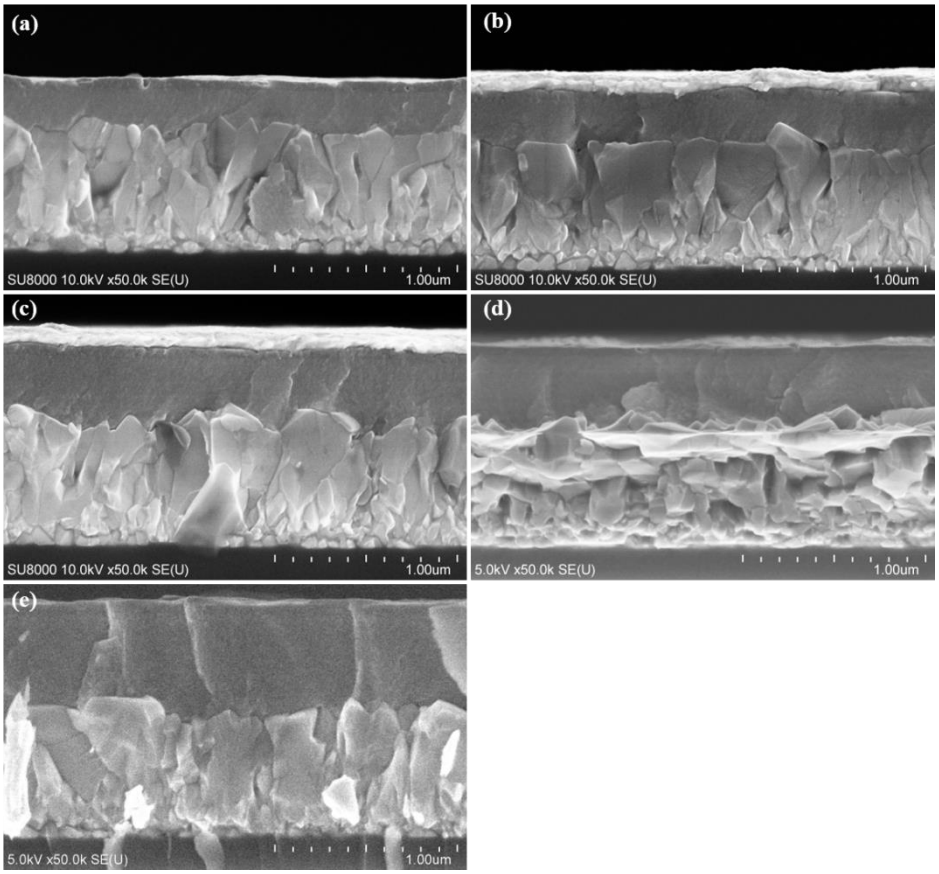

Figure S7. Cross-sectional SEM image of MOETL-free QJSCs with different thickness of PbS-PbI_2.

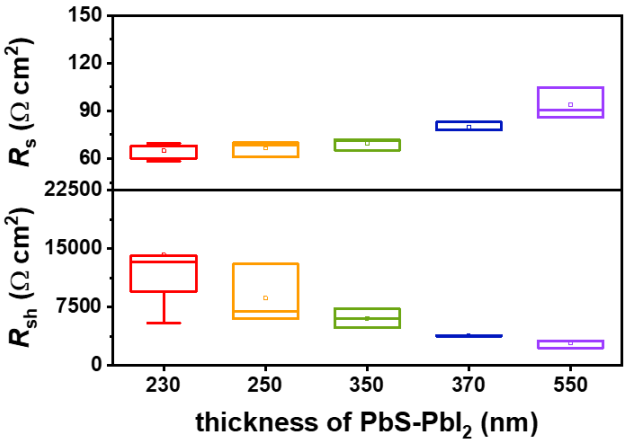

Figure S8. Series resistance (R_s) and shunt resistance (R_{sh}) for devices with different thickness of PbS-PbI_2 calculated by J–V characteristics.

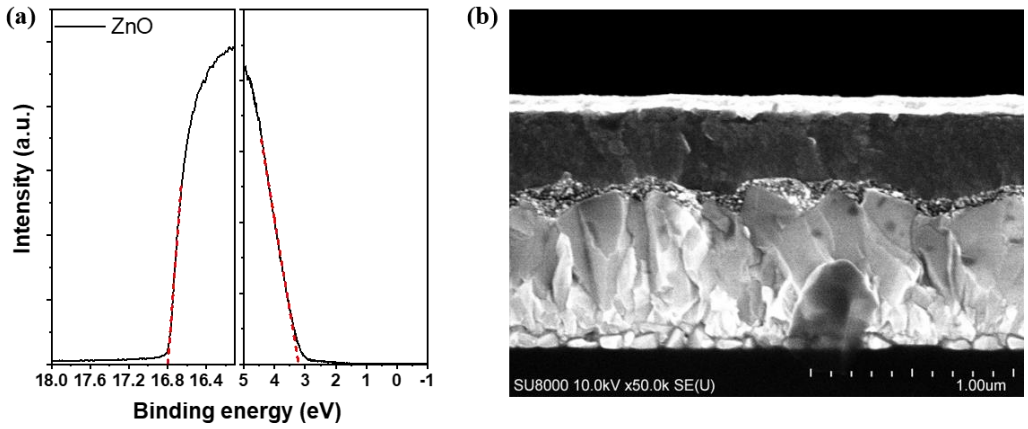

Figure S9. (a) Ultraviolet photoelectron spectroscopy (UPS) spectra of ZnO. The left side is the secondary electron cut-off region, and the right side is the near Fermi edge. (b) Cross-sectional SEM image of cell-ZnO device.

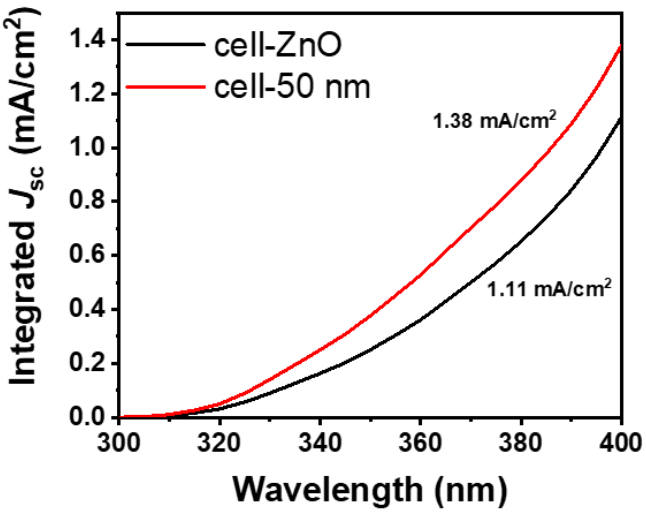

Figure S10. Enlarged EQE integrated current density image in the near ultraviolet region.

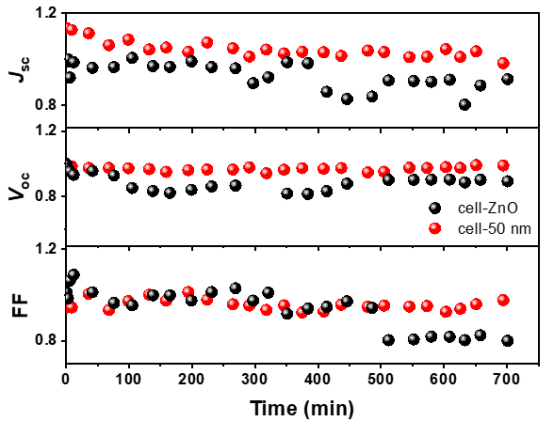

Figure S11. The J_{sc}, V_{oc} and FF of cell-ZnO and cell-50 nm as function of time. This test was carried out under the AM1.5G illumination in air ambient environment with the humidity of 30 % without temperature control.

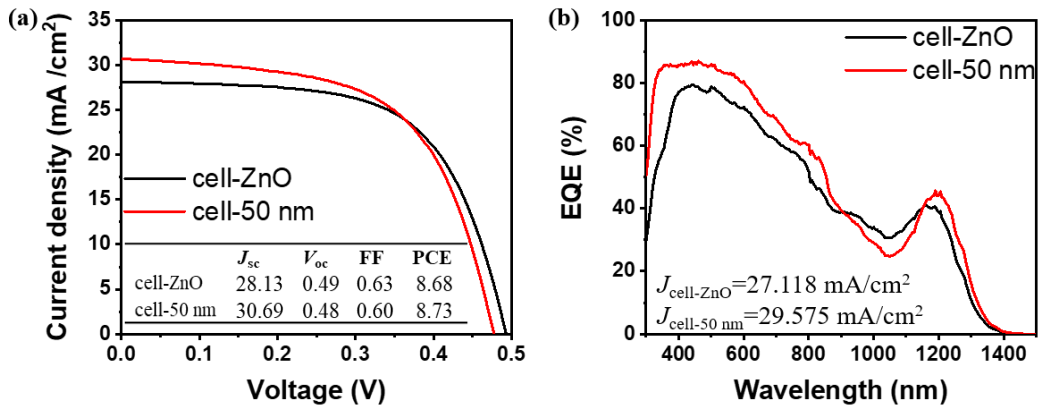

Figure S12. (a) *J–V* characteristics of cell-ZnO and cell-50 nm devices, which were fabricated using infrared PbS QDs with absorption peak of 1200 nm. (b) EQE curves of these devices.

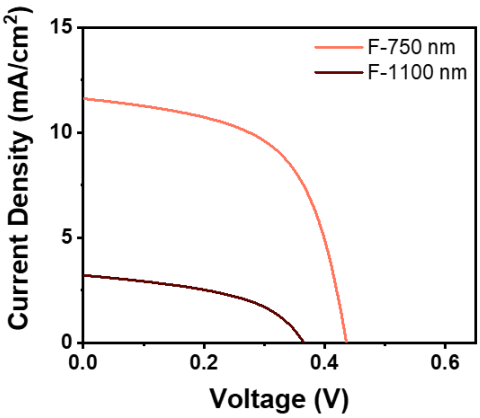

Figure S13. 750 and 1100 nm IR-filtered *J*–*V* characteristics of MOETL-free QJSCs, which were fabricated using infrared PbS QDs with absorption peak of 1200 nm.

Table S4. Performance parameters of the IR-filtered *J*–*V* characteristics.

	J_{sc} (mA/cm^2)	V_{oc} (V)	FF	PCE (%)
F-750 nm	11.62	0.436	0.580	2.93
F-1100 nm	3.21	0.366	0.472	0.55

REFERENCES

(1) Wang, H.; Kubo, T.; Nakazaki, J.; Segawa, H. Solution-Processed Short-Wave Infrared PbS Colloidal Quantum Dot/ZnO Nanowire Solar Cells Giving High Open-Circuit Voltage. *ACS Energy Lett.* **2017**, 2, 2110-2117.

(2) Takahashi, A.; Wang, H.; Fukuda, T.; Kamata, N.; Kubo, T.; Segawa, H. Annealing-Temperature Dependent Carrier-Transportation in ZnO/PbS Quantum Dot Solar Cells Fabricated Using Liquid-Phase Ligand Exchange Methods. *Energies* **2020**, 13, 5037.

(3) Brown, P. R.; Kim, D.; Lunt, R. R.; Zhao, N.; Bawendi, M. G.; Grossman, J. C.; Bulovic, V. Energy Level Modification in Lead Sulfide Quantum Dot Thin Films through Ligand Exchange. *ACS Nano* **2014,** 8, 5863-5872.

(4) Tang, J.; Liu, H.; Zhitomirsky, D.; Hoogland, S.; Wang, X.; Furukawa, M.; Levina, L.; Sargent, E. H. Quantum Junction Solar Cells. *Nano Lett.* **2012,** 12, 4889-4894.

(5) Liu, H.; Zhitomirsky, D.; Hoogland, S.; Tang, J.; Kramer, I. J.; Ning, Z.; Sargent, E. H. Systematic Optimization of Quantum Junction Colloidal Quantum Dot Solar Cells. *Appl. Phys. Lett.* **2012,** 101, 151112.

(6) Ning, Z.; Ren, Y.; Hoogland, S.; Voznyy, O.; Levina, L.; Stadler, P.; Lan, X.; Zhitomirsky, D.; Sargent, E. H. All-Inorganic Colloidal Quantum Dot Photovoltaics Employing Solution-Phase Halide Passivation. *Adv. Mater.* **2012,** 24, 6295-6299.

(7) Ning, Z.; Zhitomirsky, D.; Adinolfi, V.; Sutherland, B.; Xu, J.; Voznyy, O.; Maraghechi, P.; Lan, X.; Hoogland, S.; Ren, Y.; et al. Graded Doping for Enhanced Colloidal Quantum Dot Photovoltaics. *Adv. Mater.* **2013,** 25, 1719-1723.